fuels

MDPI

Article

The Addition of Particles to an Alternative Jet Fuel

Inês A. S. Ferrão [1,2,3], Miguel A. A. Mendes [2], Ana S. O. H. Moita [3,4,*] and André R. R. Silva [1]

1 Aeronautics and Astronautics Research Center (AEROG)—LAETA, Universidade da Beira Interior, Calçada Fonte do Lameiro 6, 6200-358 Covilhã, Portugal; ines.ferrao@ubi.pt (I.A.S.F.); andre@ubi.pt (A.R.R.S.)
2 IDMEC-LAETA, Instituto Superior Técnico, Universidade de Lisboa, Av. Rovisco Pais 1, 1049-001 Lisboa, Portugal; miguel.mendes@tecnico.ulisboa.pt
3 Centre for Innovation, Technology and Policy Research (IN+)—LARSyS, Instituto Superior Técnico, Universidade de Lisboa, Av. Rovisco Pais 1, 1049-001 Lisboa, Portugal
4 Centro de Investigação, Desenvolvimento e Inovação da Academia Militar (CINAMIL), Portuguese Military Academy, R. Gomes Freire 203, 1169-203 Lisboa, Portugal
* Correspondence: anamoita@tecnico.ulisboa.pt

Abstract: The expansion of the research on nanoscale particles demonstrates several advantages in terms of stability and an increased surface area to volume ratio compared to micron-sized particles. Based on this, the present work explores the addition of aluminum particles in hydrotreated vegetable oil (HVO), an alternative jet fuel. To evaluate the influence of particle sizes, nano and micron particles (40 nm and 5 µm) in a particle concentration of 0.5 wt.% were stably suspended in HVO. This study evaluates droplet combustion with an initial diameter of 250 µm in a drop tube furnace under different furnace temperatures (600, 800, 1000 °C). A high magnification lens coupled with a high-speed camera provides qualitative and quantitative data regarding droplet size evolution and micro-explosions. Pure HVO and Jet A-1 were also tested for comparison purposes. The results reveal that the addition of aluminum particles enhances the alternative jet fuel combustion. Furthermore, decreasing the particle size and increasing the furnace temperature enhances the burning rate compared to the pure HVO. Pure HVO presents a burning rate nearly to 1.75 mm^2/s until $t/D_0^2 = 0.35\ s/mm^2$ at T = 1000 °C. When nanoparticles are added to HVO in a particle concentration of 0.5 wt.%, an improvement of 24% in burning rate is noticed. Conventional jet fuel and pure HVO do not present any disruptive burning phenomena. However, when aluminum particles were added to HVO, micro-explosions were detected at the end of droplet lifetime, regardless of the particle size.

Keywords: single droplet combustion; aluminum particles; biofuel; micro-explosion; drop tube furnace; high-speed camera measurements

Citation: Ferrão, I.A.S.; Mendes, M.A.A.; Moita, A.S.O.H.; Silva, A.R.R. The Addition of Particles to an Alternative Jet Fuel. *Fuels* **2022**, *3*, 184–206. https://doi.org/10.3390/fuels3020012

Academic Editors: Nwabueze Emekwuru and Steven Begg

Received: 1 February 2022
Accepted: 8 March 2022
Published: 22 March 2022

1. Introduction

The interest around innovative and alternative energy sources is notorious. Metal particles have received significant attention in the combustion community due to their potential use in several applications, such as propellants, explosives, pyrotechnics, among others [1–3]. According to Dreizin [4], magnesium, aluminum, and boron are metals that present high combustion energies and thus high energy densities, which attract their adoption in various systems. Choudhury [5] developed a review based on slurry fuels defined as a suspension of fine particles of solid fuel in a liquid hydrocarbon, an advantage being its high energy density. Potential applications of coal/water and coal oil/slurry were discussed, as well as the burning characteristics of aluminum, boron, and carbon slurries. Moreover, use of micron-size particles in several applications showed issues regarding clogging, rapid settlement, poor stability, and particle agglomeration were also reported [6]. These issues are disadvantages that influence the operation of the systems.

Several researchers have demonstrated attraction to the investigation of micro-explosions that occurred in slurry fuels [7,8]. Baek et al. [7] stated that a micro-explosion appears due to the shell formation and a pressure build-up shell promoted by the suppression

of evaporation, subsequent superheating, and heterogeneous nucleation of a liquid fuel. The authors [7] also defend that these micro-explosions can reduce the corrosion of combustor walls and a few pollutant reductions derived from inefficient combustion. More recently, Valiullin et al. [9] evaluated the ignition and combustion of slurry fuel droplets under different heating conditions. In this context, conductive, convective, and radiation mechanisms were considered. The authors noticed that the minimum ignition delay times were obtained during convective heating and the maximum combustion temperatures were obtained with radiation heating.

A considerable number of experimental studies regarding metal combustion suspended or not in liquid hydrocarbons can be found in literature. However, constraints in experimental setup can complicate the research and development in this field. Due to this, numerical analysis can be a helpful complement for experimental studies, which allows the replication of complicated conditions and a better understanding of physical aspects. Several numerical approaches to evaluate the aluminum combustion [10–12], and slurry fuel droplets [13] were developed for comprehension of these subjects and also potentially helping metal combustion studies. Furthermore, numerical studies focused on aerodynamic aspects [14,15] and droplet combustion even in the absence of particles [16,17] are also relevant for the scientific community.

Previous studies were primarily based on micron-sized particles [18]. However, through research and development of nanotechnology, the possibility of obtaining particles with a smaller size and various advantages was achieved. Based on this, nanoparticles have demonstrated that their physicochemical properties are truly favorable compared to those micron-sized particles. In this respect, thermodynamic and heat transfer properties change as a consequence of the increase in surface-to-bulk atom ratio and specific surface area. Thus, a higher reactivity can be accomplished due to the increase of surface area available to react [4,6,19]. These achievements of using nanoparticles can be extended to other fields.

Nanofuels can be defined as a novel type of fuel where nanoparticles in a range of 1–100 nm are dispersed in a conventional liquid fuel. Basu et al. [20] developed a review dedicated to the combustion and heat transfer characteristics of nanofluid fuel droplets. The authors [20] stated that the addition of nanoparticles to conventional fuels and propellants improved combustion performance in terms of enhancement in volumetric energy density, catalytic activity, low ignition delay, and reduced soot and pollutant emissions. Additionally, higher ignition probability and higher burning rates were also reported. The minimization or mitigation of issues involving clogging, rapid settlement, poor stability, and agglomeration caused by micron-size particles can be solved by using nanoparticles [6].

A preliminary study involving the use of nanoparticles in conventional fuel was developed by Tyagi et al. [21]. The purpose of the study was to improve the ignition properties of diesel, adding aluminum and aluminum oxide nanoparticles in different particle sizes (15 and 50 nm) and volume fraction (0%, 0.1%, and 0.5%). Results demonstrated that the ignition probability of diesel increases when nanoparticles are added. To understand the effect of particle size, Gan and Qiao [22] performed an experimental study to evaluate the burning characteristics of fuel droplets containing nano and micron-sized aluminum particles. Several parameters were investigated, such as stability, surfactant concentration, and the type of base fuel (ethanol and n-decane). The authors observed that the particle size and base fuel influence the stability. Thus, nanoparticles suspended in a fuel present better stability when compared to micron-sized particles, and ethanol provides better suspension than n-decane fuels. In this work, micro-explosions were observed for both particle sizes. However, micro-explosions of micron-sized particles occurred later than the fuel with nanoparticles with much stronger intensity and were accompanied by intense fragmentation of the primary droplet. The occurrence of micro-explosions was also reported in various investigations [23–25]. Javed et al. [23] studied the evaporation behavior of kerosene droplets with different aluminum particle concentrations using a silicon carbide fiber. It was reported that an increase in the furnace temperature and particle

concentration leads to micro-explosions with higher intensity and earlier in the droplet lifetime. The same study [23] observed that the furnace temperature and particle concentration affect the nanofuel evaporation rate. The increase in the evaporation rate is noticed until a specific particle concentration (2.5%). The increase of the evaporation/burning rate was also noticed by Tanvir and Qiao, and Tanvir et al. [26,27]. Tanvir and Qiao [26] developed a stream droplet combustion experiment to evaluate the influence of droplet size. Aluminum nanoparticles were stably suspended in ethanol. The results reveal that adding aluminum nanoparticles in a concentration of 5.0 wt.% to the ethanol enhanced the burning rate by 140%. The authors noted that the absorption of radiation energy emitted from the stream flame is a relevant energy transfer mechanism on nanofuels. The pertinence of relation between evaporation/burning rate of a nanofuel droplet with the radiation absorption has been reported in the literature [28,29]. Gan and Qiao [29] performed an investigation of the radiation properties of nanofluid fuels and their influence on droplet evaporation rates. The work was performed using two different nanoparticles (Al and Al_2O_3) suspended in ethanol. The results reveal that radiation absorption can be significantly enhanced by adding a small amount of aluminum nanoparticles to the base fluid. Furthermore, comparing the influence of Al_2O_3 and Al nanoparticles in ethanol, it was demonstrated that the former reduces radiation absorption. In general, the strong absorption of radiation energy by nanoparticles increases the nanofluid droplet temperature, leading to an enhancement in the evaporation process. It is proved that the addition of nanoparticles can potentially improve certain combustion characteristics of liquid fuels. In this context, refs. [30,31] evaluated the jet fuel combustion with various type of nanoparticles.

According to Ng et al. [32], aviation fuels can be designated as commercial and military jet fuels. Regarding the commercial jet fuel, Jet A is used in the United States while most of the rest of the world uses Jet A-1, the freezing point being the main difference [33]. For military aviation, JP-8 is the fuel mainly used. Conventional jet fuels are provided from kerosene produced from crude oil, a finite source. Fossil fuels are the main energy source globally and have limited resources. In addition, products of fuels used in aviation negatively impact the environment. The aviation concerns in terms of depletion of fossil fuels, allied with the accelerated growth of this sector and the emissions of greenhouse gas and pollutant, have forced more ecological and sustainable solutions. A potential pathway to solve these issues is the employment of biofuels due to their sustainability and the possibility of using them in aero-engines. Furthermore, biofuels are promising fuels that can replace fossil fuels and reduce pollutant emissions. These fuels are renewable sources derived from organic matter, which may include firewoods, animal fats and oils, charcoals, animal dungs, and vegetable oils [34]. The introduction of biofuels or alternative jet fuels has already been investigated and in this respect should comprise several properties, such as inedible, renewable resources, reduced pollutant, and greenhouse gas emissions, compatibility with the traditional fuel, sustainability, and clean burning [35,36]. According to [37], a few categories and technology pathways were approved by the American Society for Testing and Materials (ASTM). Hydroprocessed esters and fatty acids (HEFA) technology use vegetable and waste oils that are available to be produced on a large scale and were already used in commercial passenger flights [36,37].

As mentioned above, the use of biofuels and enhancing their performance with particle additives is a relevant topic for combustion systems. Thus, this study evaluates the effect of particle size in alternative jet fuel (HVO/HEFA), a biofuel already tested and used in real aero-engines. To accomplish this, a free falling droplet combustion will be studied under the influence of three furnace temperatures (600, 800, 1000 °C). Additionally, conventional jet fuel and pure biofuel were also tested. In the literature, nanofuels or micron-sized particles suspended in liquid hydrocarbon studies using a small droplet diameter are scarce. Moreover, the use of a supportive fiber was also avoided to better understand the onset of disruptive burning phenomena. The present work provides a satisfactory compromise between experimental work and practical conditions due to the use of relatively high

furnace temperature, reduced droplet diameter, and no supportive fiber, which can offer a new perspective in this field.

2. Materials and Methods

2.1. Fuels Preparation and Properties

In the present work, conventional jet fuel (Jet A-1) and a biofuel (HVO) were tested for comparison purposes. Table 1 shows the HVO and Jet A-1 properties. Jet fuel powered aircraft engines differ from the traditional combustion engine fuels, mainly in their physicochemical properties, due to restrictions imposed by the aeronautical industry to guarantee reliability, safety, security, and other aspects. It requires a high energy content, good flow characteristics, and thermal stability [38]. Commercial aviation fuel (Jet A-1) is supplied from kerosene and derived from a fractional distillation of crude oil. This fuel is a mixture of many different hydrocarbons being mainly composed of n-paraffins, branched iso-alkanes (iso-paraffins), cyclic alkanes (naphthenes), and aromatics [32,39]. Hydrotreated vegetable oil (HVO) or HEFA is a renewable fuel obtained from converting vegetable oils and animal fat into paraffinic hydrocarbons. This alternative jet fuel is a NExBTL from NESTE that presents a high cetane number and does not contain sulfur, aromatics, and oxygen in its composition. These fuels are stable for storage, resistant to microbial growth, and do not form deposits in engines. According to [35], these are suitable for conventional aircraft engines without further engine modification and do not raise any fuel quality issues. In agreement with ASTM D7566 specification, HVO can be mixed with conventional jet fuel, up to a blend ratio of 50% [39].

Table 1. HVO and Jet A-1 properties adapted from [32,33,40,41].

Parameter		Standard Limit	Jet A-1	HVO
Density (kg/m^3) (at 20 °C)		771–836	798	780.6
Kinematic viscosity (mm^2/s) (at 25 °C)			1.40	4.33
Surface tension (N/m) (at 20 °C)			0.0247	0.0265
Distillation	10 vol.% (°C)		170	262
	50 vol.% (°C)		189	279
	90 vol.% (°C)		219	291
	Final boiling point (°C)	Max. 300	237	308
Flash point (°C)		Min. 38.0	38	77
Cloud point (°C)			−26	−34
Sulfur (wt.%)		Max. 30.0	0.3	0.09
Aromatics (wt.%)		Max. 25.0 (vol.%)	13.8	0
Lower heating value (MJ/kg)		Min. 42.8	43	43.9
Higher heating value (MJ/kg)			47	47.1
Hydrogen content			14.5	15.4
Carbon content			84.6	85.5
H/C ratio			1.91	2.18
Carbon number			C8–C16	C15–C18

Figure 1 shows the distillation curve for the biofuel (HVO) and the conventional jet fuel (Jet A-1). The HVO presents a higher boiling point when compared to the Jet A-1. Additionally, it also displays a narrow boiling point range. This observation can be attributed to the fact that HVO biofuel consists mainly of saturated hydrocarbons having 15 to 18 carbon atoms in their molecules [42]. On the other hand, aviation fuel comprises C8 to C16 hydrocarbon molecules, reflecting a broad distillation curve.

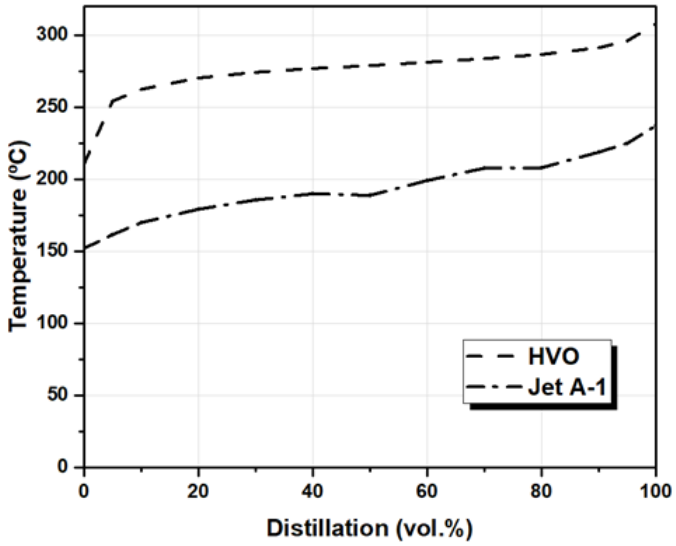

Figure 1. Distillation curve for Jet A-1 and HVO.

In the present work, the metal particles used were aluminum as a result of high density, high heat release during oxidation, relatively low cost, safe to use, and abundance in Earth [1]. Micron- and nano-sized aluminum particles were used in various studies reported in the literature, providing insight regarding this subject and data for comparison purposes. It is also important to highlight that no particle oxidation was noticed when added to HVO, which is why this biofuel can be evaluated with aluminum particles. A low particle concentration of 0.5 wt.% and two particle sizes (40 nm and 5 µm) were considered to evaluate the influence of adding aluminum particles to the biofuel. A reduced particle concentration was used in order to guarantee the samples stability during the experiments. The particle sizes were defined based on literature findings [6,22]. It is essential to mention that the main purpose for comparing nano- and micron-sized particles. Figure 2 shows SEM images of aluminum particles for (a) 40 nm and (b) 5 µm. Supplementary images of the particles produced from Nanografi were added in Figure A1. Figure 3 shows the fuels tested in this work. The pure fuels, HVO and Jet A-1, are essentially transparent fluids. However, when aluminum particles are added to the base fuel, it is perceived that the sample becomes dark and opaque, consequently influencing the radiation absorption.

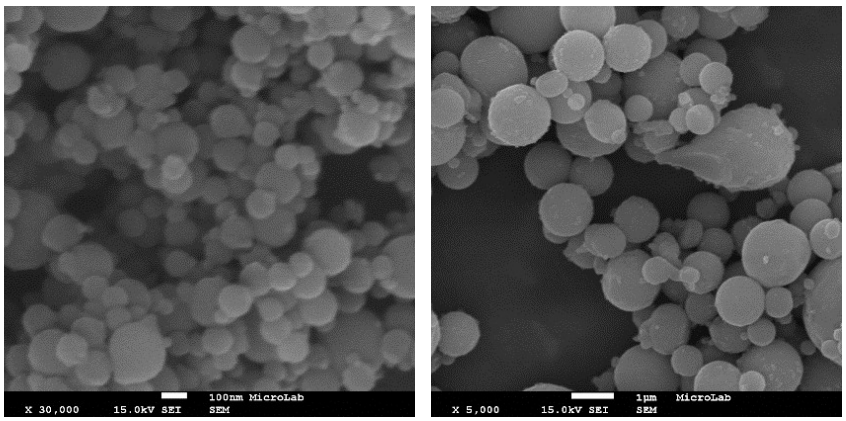

Figure 2. SEM images of aluminum particles (**a**) 40 nm and (**b**) 5 µm.

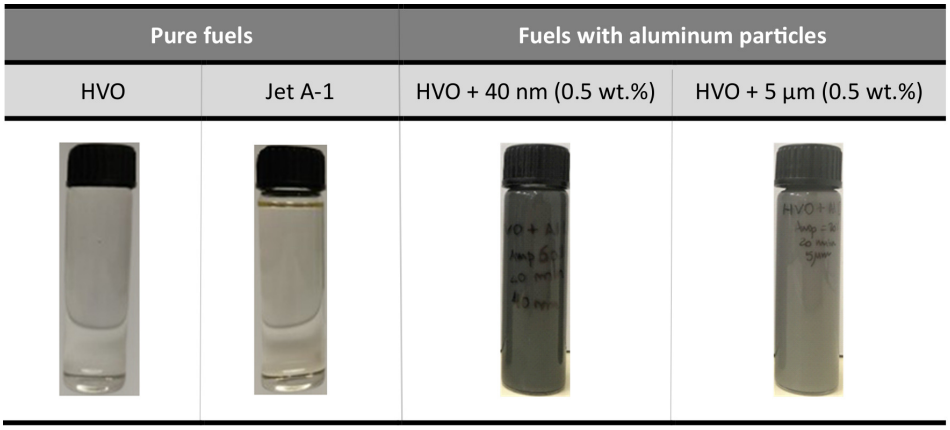

Figure 3. Fuels tested in the present work: HVO; Jet A-1; HVO + 40 nm (0.5 wt.%); and HVO + 5 µm (0.5 wt.%).

The preparation of HVO + Al particles required a methodic procedure, an introductory phase in studies that evolved a stable suspension of particles in liquid fuel. As mentioned, two particle sizes (40 nm and 5 µm) and a particle concentration of 0.5 wt.% were considered. According to [43] in nanofluids, the Brownian motion and nanoparticle aggregation are the dominant mechanisms for the rheological properties compared to the micron-sized suspensions. The development and growth of agglomeration and clogging can affect the physical properties [44]. Due to this, the sample should be homogeneous and stable with no evident particle agglomeration before and during the experiments [22]. A two-step method was applied to evaluate the stability, and a qualitative study based on visual inspection was performed.

Firstly, a precise mass of HVO and particles was mixed for 20 min with magnetic stirring. Then, the liquid fuel with particles was sonicated in an ice bath for 30 min to disperse the particles and avoid agglomeration. Afterward, the nanofuels stability is examined in a test tube for several hours, days, and weeks. Figure 4 shows nanofuel stability results. Sample A corresponds to a stable suspension, and sample D corresponds to an unstable suspension, where most of the particles are presented at the bottom of the test tube. Therefore, it was concluded that nanofuel stability reduction is noticed as time evolves. Additionally, diminishing stability is observed as the particle size increases. In this context, the HVO + 40 nm is more stable than HVO + 5 µm. Yetter et al. [19] reported that micron-size particles after the dispersion settle very quickly when compared with nano-size particles. Thus, nanoparticles present small mass, diameter, and specific surface area, allowing the suspension for a considerable amount of time under certain conditions. It is essential to highlight that the samples were stable during the single droplet combustion experiments. In the present work, the use of surfactants was negligible. However, adding a surfactant to this novel type of fuel is essential to enhance the stability for higher particle concentration and large particle sizes. Moreover, the influence of surfactants should be evaluated in terms of pollutant emissions and combustion characteristics to understand if they affect the droplet combustion dynamics.

Figure 5 shows the physical properties of Jet A-1, pure HVO, HVO + 40 nm (0.5 wt.%), and HVO + 5 µm (0.5 wt.%). The horizontal red dashed line corresponds to the Jet A-1 (conventional aviation fuel). The black dashed-dotted line corresponds to the pure HVO. Density is depicted in Figure 5a, surface tension in Figure 5b, and lastly viscosity in Figure 5c. The density was measured at room temperature (20 ± 3 °C) with Densimeter DA-130N, and surface tension was measured with an optical tensiometer THETA (Attension), using the pendant drop method. A detailed description of the measurement procedures is provided elsewhere [45]. Regarding the viscosity, Brookfield DV3TRVCP Rheometer was used, and its accuracy is ±1.0% of the range. It was observed that the viscosity presents the major difference between pure HVO and Jet A-1. No significant alter-

ation of the physical properties of HVO + Al particles at this specific particle concentration, compared to pure biofuel, was noticed. Tanvir and Qiao [46] argue that at low particle concentration, the addition of particles has little influence, as observed in surface tension, due to the large distance between particles.

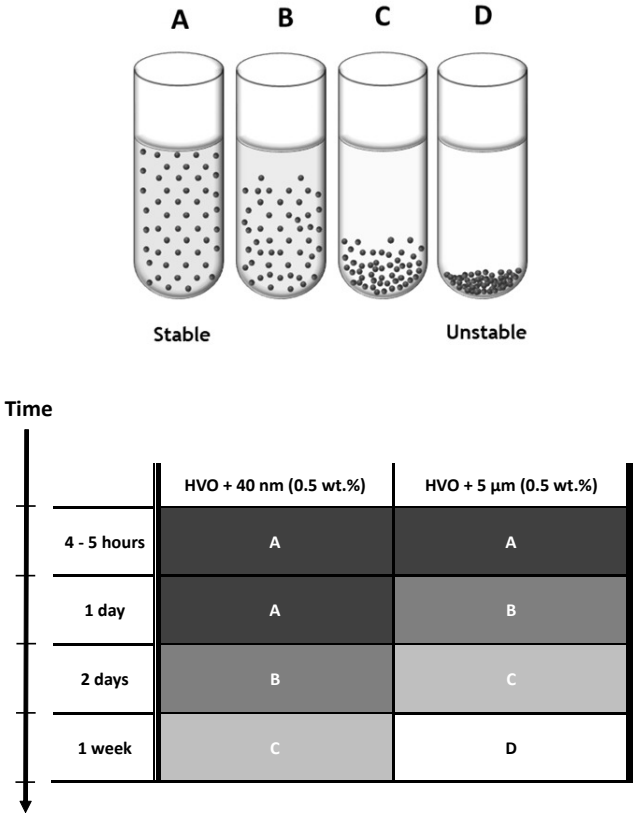

Figure 4. Stability study.

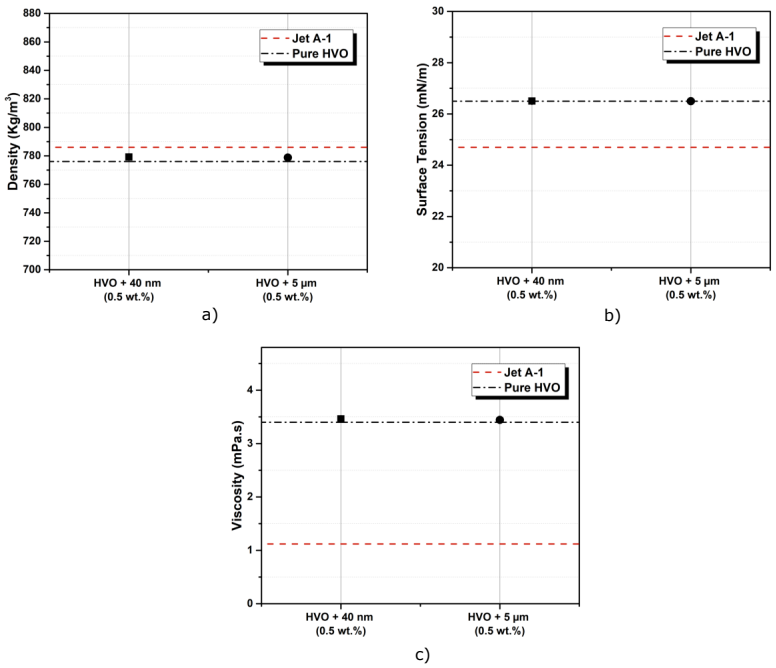

Figure 5. Physical properties of the fuels used in the present work, (**a**) density, (**b**) surface tension and (**c**) viscosity.

2.2. Experimental Setup

Figure 6 shows a schematic of experimental setup. The main elements of the experimental facility are: drop tube furnace (DTF), illumination setup, image acquisition, and droplet injection system. The DTF is heated by electric coils and allows the control of the wall temperature and oxygen concentration, capable of achieving a maximum temperature of 1200 °C. A vertical quartz tube is placed inside the DTF and possesses an inner diameter of 6.6 cm and a length of 82.6 cm. A water-cooled injector at the top of the DTF was used to feed the droplet and the oxidizer to the quartz tube. Thus, droplet combustion occurs inside the quartz tube in a falling droplet method. The water-cooled injector allows the entrance of the air supply to generate suitable surroundings for the droplet autoignition and combustion. The air enters at the injector with a flow rate of 5.7 L/min and a precision error of ±2%. Therefore, the injector has a distinct inlet for the air supply and the single droplets. When the quartz tube environment reaches the desired temperature for each test condition, the injection of a single droplet occurs. This experimental setup allows the droplet combustion in a stable atmosphere, being the droplet trajectory in the central axis of the quartz tube [41]. Figure 7 shows the temperature profile along the quartz tube for the three test temperatures (600 °C, 800 °C, 1000 °C). These high furnace temperatures allow an acceptable compromise between experimental and practical conditions. The data were acquired using a 76 µm diameter fine wire platinum/platinum: 13% rhodium (type-R) thermocouple. The horizontal axis corresponds to the distance from the tip of the injector (x = 0 cm). The maximum standard deviation was T = 800 °C ± 56 °C at x = 0 cm.

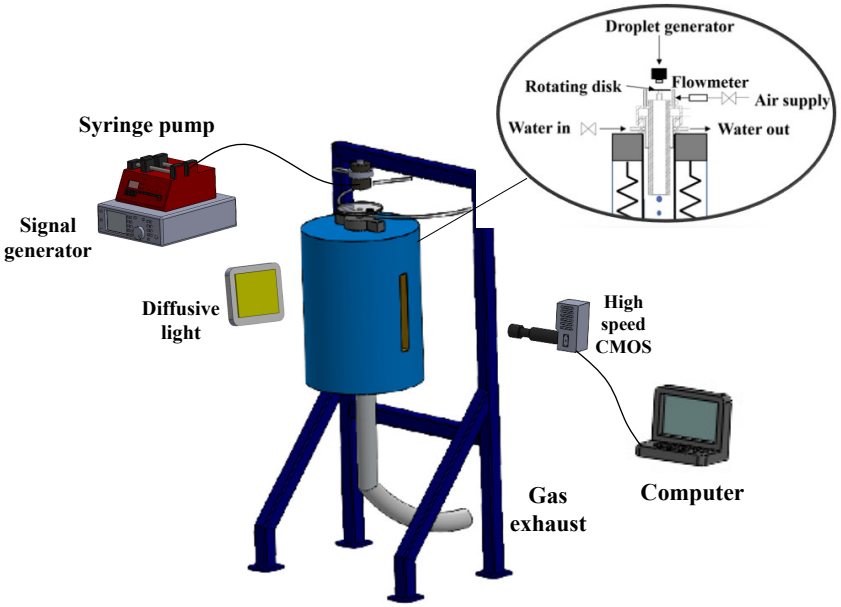

Figure 6. Droplet combustion experimental setup.

The droplets are injected by a system with a syringe pump, frequency generator, and droplet generator. A TSI device, a commercial droplet generator, is placed at the top of the DTF. A pinhole with a diameter of 200 µm is coupled to the droplet generator producing a droplet stream. The fuels are fed with the aid of a syringe with a volume of 50 mL being connected to a syringe pump. The operating conditions of the droplet dispensing system are approximately 2.1 kHz and a flow rate of 1.3 mL/min, releasing a stream of droplets with an initial diameter of 250 ± 12 µm. To this system, a rotating disk was also added to guarantee the space/time between droplets. The rotating disk presents approximately a diameter of 12 cm and a rotational speed of 1200 rpm with a 1 cm × 1 cm slot. This rotating disk apparatus ensures no interferences from the droplet–droplet interaction in this study. The literature states that droplets spaced at least 30 diameters apart could ensure independent burning [47,48]. Subsequently, each analysis was performed

with approximately 50–60 droplet diameter distance. Additionally, the DTF has two opposite rectangular windows with 2 cm width and 20 cm height for the droplet combustion visualization. The illumination set is displayed opposite from the image acquisition system. The illumination set comprises an LED light and a diffusion glass to improve the contrast and fully visualize the droplet size evolution and disruptive burning phenomena. Regarding the image acquisition system, a CMOS high–speed camera (CR600×2 from Optronis GmbH, Ludwigstr. 2, 77694 Kehl, Germany), coupled with a high magnification lens, was used. This system is connected to a computer, with the camera being manually triggered. The magnification lens is composed of a 6.5× Zoom, 12 mm FF, a 0.25× lens attachment, and a 2.0× short adapter, with a magnifying range of 0.35–2.25, leading to an increase in the spatial resolution of the image up to 8.2 µm/pixel. The image acquisition was pursued with 1000 fps with a resolution of 1200 × 500 pixels and an exposure time of 1/13,000 s. To visualize disruptive burning phenomena in more detail, a high speed camera Photron FASTCAM mini UX50 with 1.3 Megapixel was used with a high magnification lens. In these particular observations, the image acquisition was performed with 3200 fps and a exposure time of 16,000 s. Additional images of the experimental setup are provided in Figures A2 and A3.

Firstly, the nanofuel preparation is performed. Subsequently, the droplet combustion after the test temperature is achieved and several images are recorded. The last step corresponds to the images analysis. The image data processing was performed in ImageJ and MATLAB software. The ImageJ software evaluated the droplet size evolution, burning rate, and droplet velocity. A region of interest (ROI) is defined, and the droplet outline is marked through the brightness gradient for these analyses, allowing the droplet characterization. The identification of puffing and micro-explosions was performed in the MATLAB software through an algorithm developed. The image data processing was performed using subtraction, binarization, and identification of elements in the recorded images. As mentioned in a previous study [49], in order to guarantee that the droplet size evolution and burning rate of each fuel were independent of the sample size, a statistical study was performed. Thus, the number of droplets that were essential to elaborate the results was investigated. The study reveals that a minimum of 35 droplets is required to achieve a statistical convergence, where no significant variation in the droplet size evolution curves and burning rate were noticed. Therefore, 40 droplets were considered to each droplet size evolution curve, as will be described in the following section.

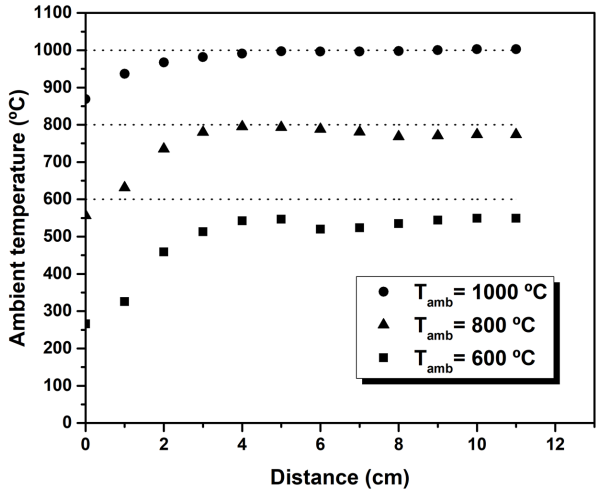

Figure 7. Temperature profile along the quartz tube.

3. Results

3.1. Visualization and Description of Pure Fuels Combustion

This section is dedicated to single droplet combustion of Jet A-1 and pure HVO. Droplet size evolution, burning rate, and flame intensity will be compared for the test furnace temperatures. As previously mentioned, three furnace temperatures (T = 600, 800, 1000 °C) were considered. The experiments for each fuel were performed under all temperatures, however, for T = 600 °C, no quantitative results are described in the present work. At the lowest furnace temperature, regardless of the fuel, the visualization and identification of auto-ignition were not possible in the majority of the droplets. In this context, to provide an accurate comparison in all operating conditions, the droplet size evolution and the burning rate at this specific temperature will not be analyzed and explained in detail. Droplets were injected in the quartz tube after the desired test temperature was achieved, as shown in Figure 7. The air is introduced in the quartz tube and heats due to the electric coils presented in DTF. The droplet begins to vaporize from its surface when entering the hot environment. Consequently, auto-ignition occurs immediately upon fuel vapor, and air mixing is in an adequate proportion, leading to a diffusion flame formation. In addition, ignition delay was not evaluated in the present work due to the constraints in the experimental setup.

Figure 8 shows the droplet size evolution for Jet A-1 and HVO coupled with the visualization of single droplet combustion. Figure 8a shows the square of the normalized droplet diameter (D^2/D_0^2) as a function of the normalized time (t/D_0^2). Each curve was developed using 40 droplets, and a five-point moving average was employed for the smoothening purpose. The results show that conventional jet fuel and biofuel obeyed the D^2 law. Therefore, the normalized square diameter decreases linearly with a nearly constant rate defined as burning rate (K). Droplets of pure HVO display a longer lifetime, however normalized droplet diameter evolution is quite similar for most of the lifetime compared with Jet A-1. The major difference between the fuel is noticed at the end of the droplet lifetime. It is essential to mention that the auto-ignition of Jet A-1 occurs at a smaller distance from the tip of DTF injector related to the HVO. This fact can be attributed to compounds with lower boiling points (lighter compounds) present in Jet A-1 composition [50]. As displayed in Figure 7, at T = 800 °C the droplet ignites in the region between x = 3 and x = 4 cm. The maximum standard deviation in droplet size evolution curve at T = 800 °C for Jet A-1 was ± 0.05 and for HVO it was ± 0.08.

Jet A-1 and pure HVO do not present any disruptive burning phenomena in the droplet lifetime. Figure 8b shows instantaneous images of burning droplets at different instants. It can be observed that as time evolves, the droplet diameter reduces as described in Figure 8a for both pure fuels. An important characteristic that emerges among fuels is flame intensity. In the present work, the visualization indicates that no symmetric spherical flame is noticeable. Due to the high aromatic content, a brighter flame is noticed for Jet A-1 [51]. On the other, the identification of HVO flame is quite difficult, and as mentioned earlier, the biofuel does not possess aromatics in its composition and displays a flame with lower intensity. In short, the flame intensity decreases as the droplet shrinks along its lifetime, as depicted in Figure 8b.

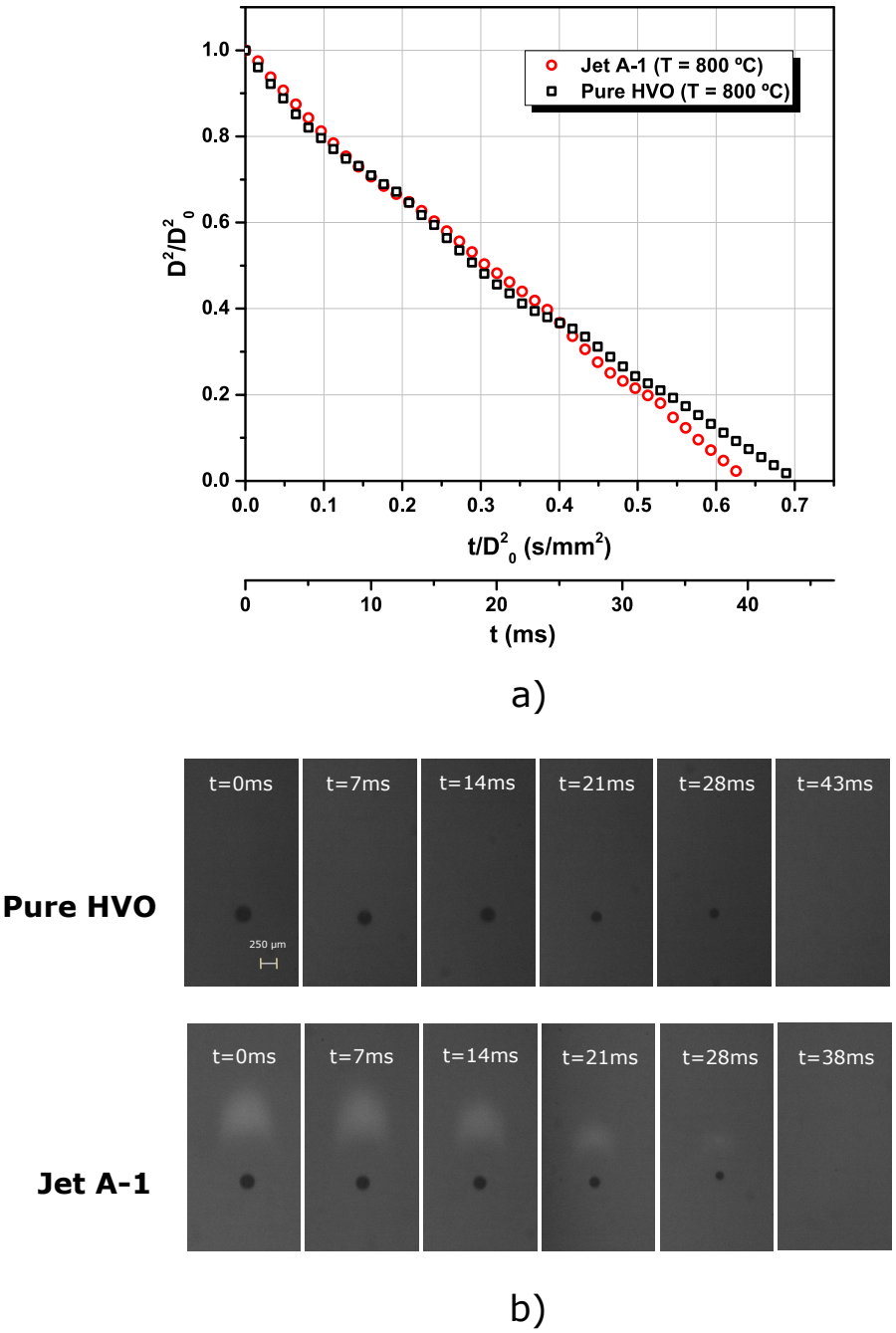

Figure 8. Jet A-1 and HVO combustion at T = 800 °C: (**a**) Droplet size evolution; (**b**) Sequence of imagens of burning fuels.

Figure 9 shows (a) droplet size evolution and (b) visualization of droplet combustion at T = 1000 °C. Similarly to T = 800 °C, the fuel is in good agreement with D^2 law. The normalized square diameter decreases linearly with time without the occurrence of any disruptive burning phenomena. The results show that by increasing the furnace temperature, the combustion of fuels becomes closer.

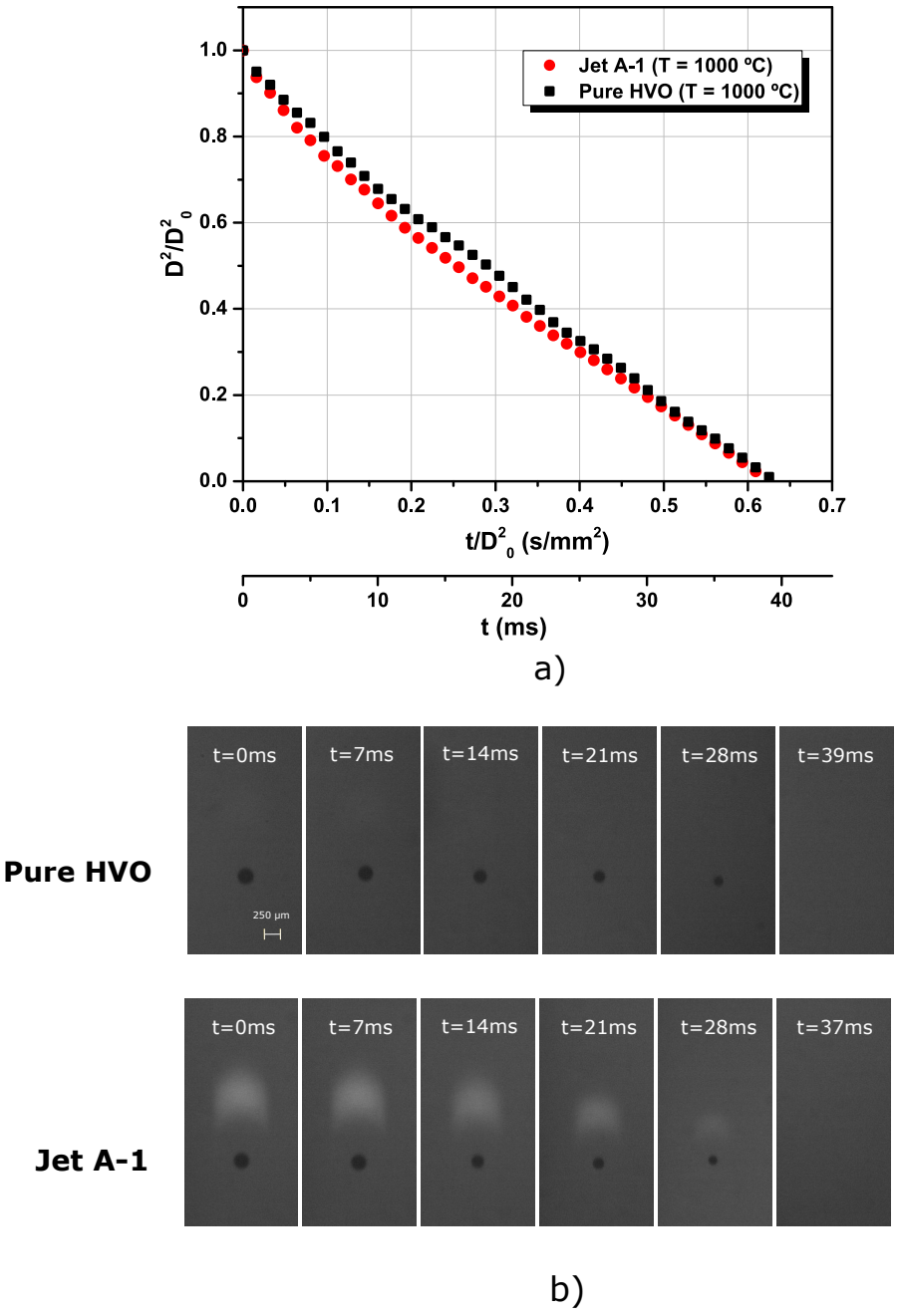

Figure 9. Jet A-1 and HVO combustion at T = 1000 °C: (**a**) Droplet size evolution; (**b**) Sequence of imagens of burning fuels.

Figure 9a shows that droplet size evolution and lifetime are quite similar for both fuels. The maximum standard deviation in droplet size evolution curve at T = 1000 °C for Jet A-1 was ±0.06 and for HVO it was ±0.08. Figure 9b shows the sequences of instantaneous images of burning droplets at 1000 °C of the pure HVO and Jet A-1. At T = 1000 °C, the droplet size reduces when the time increases, as observed for T = 800 °C, and Jet A-1 presents the brighter flame. According to the literature, a reduction in pollutant emissions is reported when HVO is used. It also reported a behavior not so different from Jet A-1 and HVO [49,51–53]. Figure 10 shows the droplet velocity at a different furnace temperature, (a) T = 800 °C and (b) 1000 °C. Firstly, the droplet velocity was determined by the centroid position for two sequential frames divided by the time between the two frames. Afterwards, it employed a polynomial function to the experimental data points in order to obtain velocity curves for both pure fuels in the two furnace temperatures. At the

early stages, where D^2/D_0^2 is between 1.0 and 0.7, HVO droplet velocity is slightly higher than Jet A-1, however, as the droplet diameter is reducing the velocity tendency is quite similar, regardless of furnace temperature. The maximum standard deviation in droplet velocity at T = 800 °C was ±0.2 m/s and at T = 1000 °C was ±0.1 m/s.

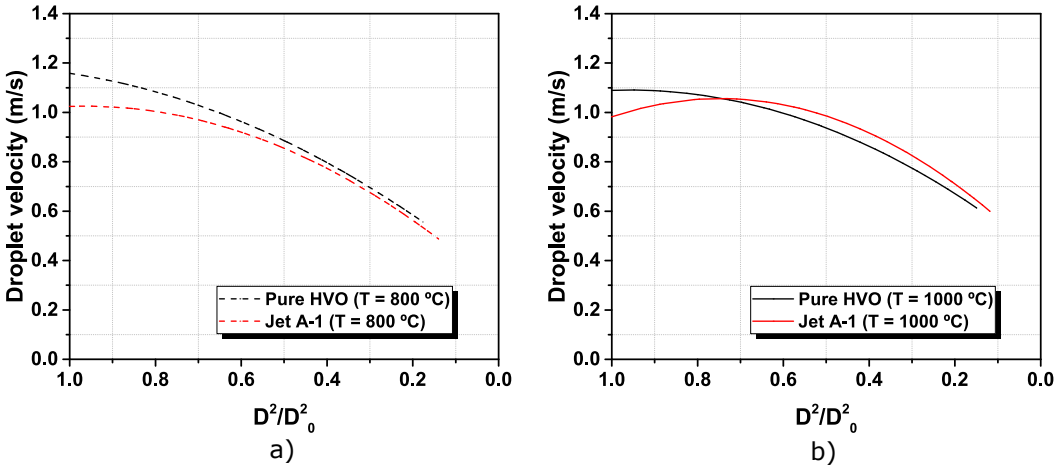

Figure 10. Droplet velocity as a function of the normalized droplet diameter at (**a**) T = 800 °C; (**b**) 1000 °C.

Studies involving droplet evaporation and combustion are a pre-requisite for improving comprehension regarding spray combustion, an essential phenomenon in several applications such as gas turbines and diesel engines. In this context, evaluating the droplet size evolution allows investigating how fast the liquid evaporates, which can be defined as burning rate. This characteristic is relevant to perceive the performance of the fuel in engine operating conditions. Figure 11 shows the burning rate for Jet A-1 and HVO at (a) T = 800 °C and (b) T = 1000 °C. The horizontal lines correspond to the final burning rate, considering the entire droplet lifetime. Red and black lines are related to the Jet A-1 and HVO, respectively. In this context, the burning rate is determined through $K = -d(D^2)/dt$. At T = 800 °C, Jet A-1 has a higher burning rate (1.51 mm^2/s) compared to pure HVO (1.41 mm^2/s). Increasing the furnace temperature increases the final burning rate, and it has noted proximity in these values for the pure fuels, as shown in Figure 11b. Regarding the temporal evolution of the burning rate, the results demonstrate that liquid fuel is evaporating without any significant disturbance, leading to an approximate constant burning rate value, regardless of furnace temperature.

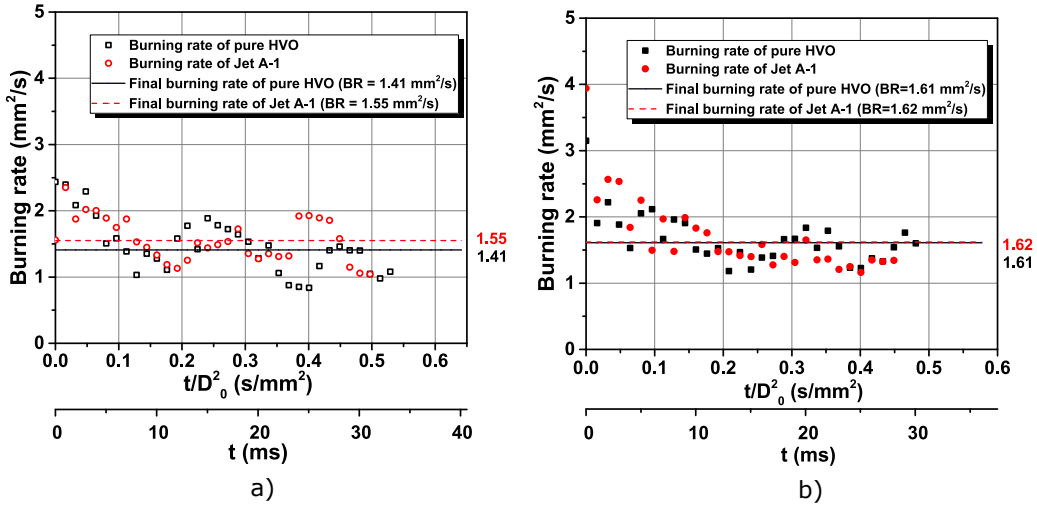

Figure 11. Temporal evolution of burning rate and final burning rate for the Jet A-1 and pure HVO at (**a**) T = 800 °C and (**b**) T = 1000 °C.

3.2. The Addition of Particles to an Alternative Jet Fuel

The previous section described the combustion of pure HVO and Jet A-1. It was noticed that HVO provides satisfactory results; however, it is important to introduce biofuels in aero-engines to achieve a sustainable world. Thus, aluminum particles were added to the biofuel to enhance its performance, potentially decreasing fuel volume usage and increasing fleet-wide energy efficiency. To understand how different particle sizes affect the combustion of HVO, this work will provide visualization and a detailed description in terms of droplet size evolution and burning rate of alternative jet fuel with nano- and micron-sized particles.

Figure 12 shows the sequences of instantaneous images of burning droplets at different instants and furnace temperatures. The sequence of images shows that the droplet diameter is reducing as time evolves. The droplet flame has lower intensity due to the lack of aromatics content in HVO. In addition, increasing the furnace temperature increases the flame intensity, regardless of particle size. For the two furnace temperatures and particle sizes, micro-explosion appears due to the presence of particles in the biofuel. Thus, in these experiments, the probability of a micro-explosion outcome is 100% at this specific particle concentration for nano- and micron-sized particles. The appearance of micro-explosions as a consequence of adding particles to a liquid fuel was reported in several studies [22,23]. Most studies involving nanofuels or micron-sized particles stably suspended in a liquid fuel are developed in a fiber suspension technique [20,54,55]. This experimental method can act as a nucleating surface, promoting a heterogeneous boiling related to a certain low degree of superheat. Consequently, a continuous bubble formation potentially leads to a disruptive burning phenomenon [20]. Thus, the present work confirms that without using the suspended droplet method, disruptive burning phenomena can be detected due to the addition of particles. Guerieri et al. [56] developed a study using a falling droplet method, using aluminum additive and observed explosive events. Disruptive burning phenomena are characterized by two outcomes: puffing and micro-explosion. Prior to the micro-explosion occurrence, puffing is noticed. The micro-explosions correspond to the disintegration of the primary droplet, while on the other hand, puffing in most studies involving emulsions is defined as the release of volatile components [17,41]. After the droplet enters the quartz tube, the liquid fuel begins to be consumed. As the fuel liquid is evaporating, a considerable amount of particles remain inside the droplet since no obvious particle expulsion was observed during most of the droplet lifetime.

Due to this, the particle concentration increases preferentially at the droplet surface caused by the exchange of heat and mass transfer [49]. Subsequently, particle agglomeration can hinder vaporization, leading to the local hot spots. These hot spots induce biofuel vapor nucleation, leading to a micro-explosion and ejection of intense bright spots in several directions [57]. As time evolves, the solid phase becomes predominant within the droplet. Accordingly, disruptive burning phenomena are interesting in this novel class of fuels to induce secondary atomization. Liquid and solid phases will be dispersed, enhancing fuel/air mixture, reducing the droplet lifetime, and improving combustion efficiency [17,41]. Besides the fact that both particle sizes display micro-explosions, HVO + nano-sized particles seem to disperse better than micron-sized particles, however the latter possesses micro-explosions with a higher intensity which can be related to the particle agglomeration. Gan and Qiao [22] reported that micron suspension forms a densely packed, impermeable shell and nanosuspension a porous, more-uniformly distributed spherical aggregate that affects droplet evaporation and combustion. However, more studies focusing on particle agglomeration during droplet combustion should be performed to fully understand how it can affect these events. After the micro-explosion, particle agglomerates are dispersed in the quartz tube environment and are projected from the explosion region and burn. The aluminum combustion characterizes this final event. The residue derived from this final event is violently projected away, ending up ascending as the smoke tail, also reported by [49]. However, due to limitations on the experimental setup, the combustion residue was not collected. Figure 13 shows micro-explosion appearance

at T = 1000 °C for HVO + 40 nm (0.5 wt.%) and HVO + 5 μm (0.5 wt.%). This sequence of images was acquired at 3200 fps in order to enhance the outcome visualization and understanding of phenomenon explanation.

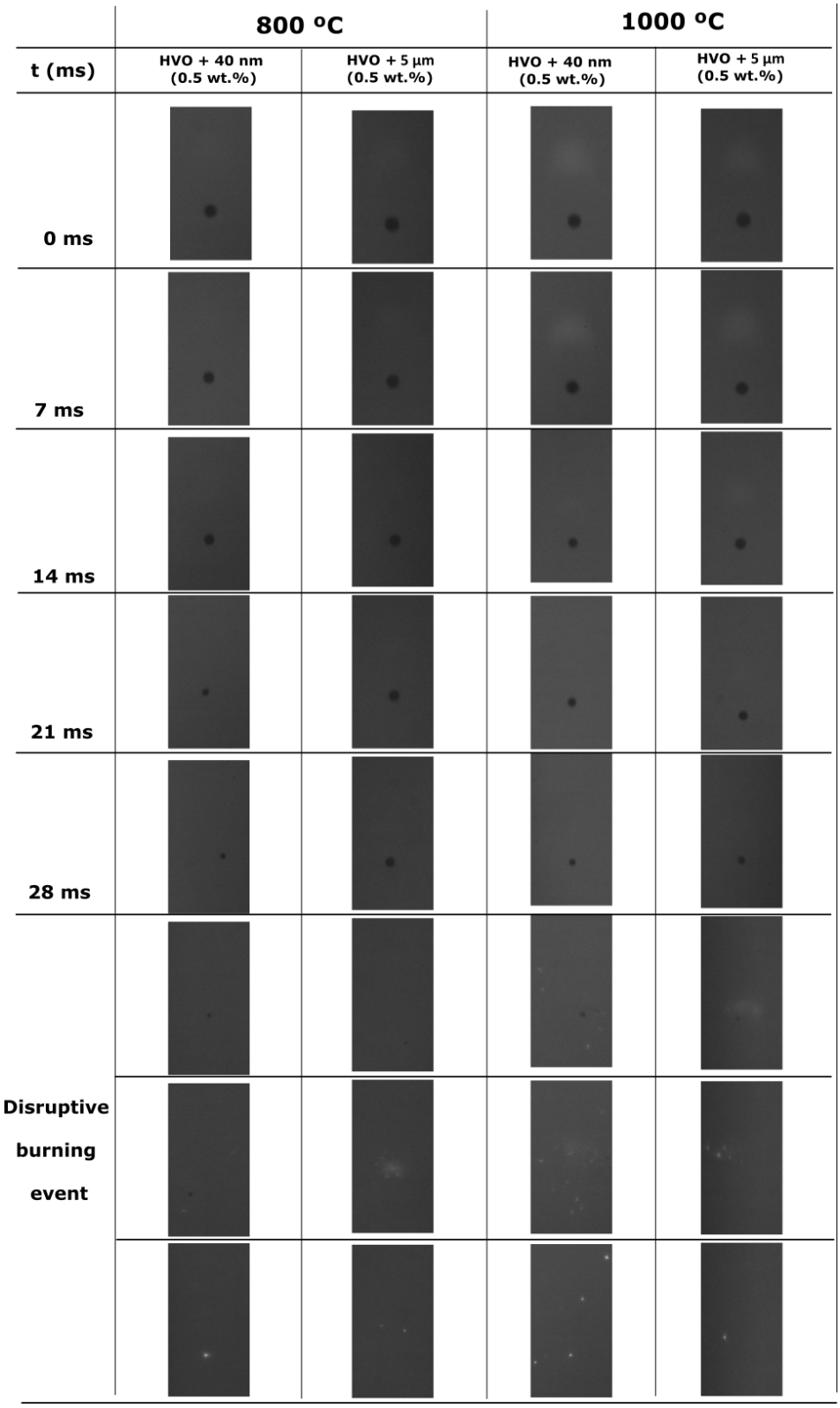

Figure 12. Sequences of instantaneous images of burning droplets HVO + Al particles.

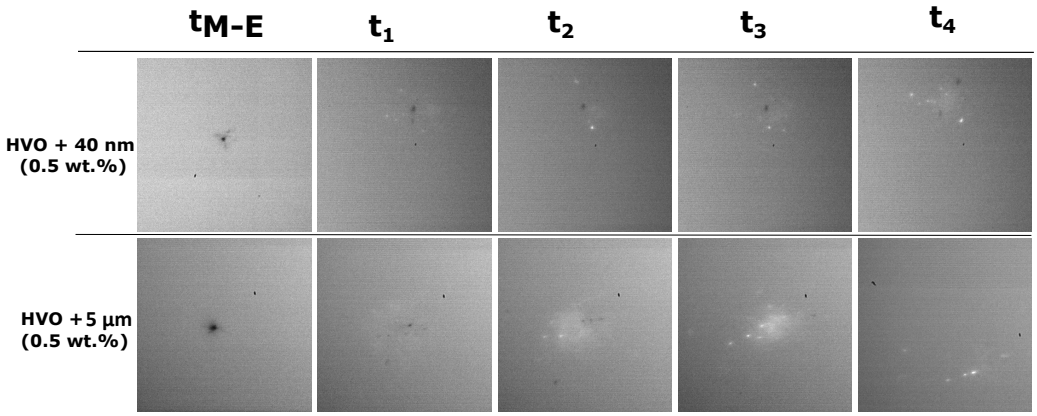

Figure 13. Micro-explosion for HVO + 40 nm (0.5 wt.%) and HVO + 5 µm (0.5 wt.%).

Figure 14 shows the normalized droplet diameter as a function of the normalized time for HVO + Al particle at (a) T = 800 °C and (b) T = 1000 °C. The droplet size evolution of HVO with aluminum particles differs from pure HVO. Pure HVO presents a steady burning, however HVO + Al presents a dry-out phase, where the droplet diameter does not reduce linearly with time. A previous study [49] reported that nanofuels display a dry-out phase at the end of the droplet lifetime, where micro-explosion occurs. A reduction of the burning rate identifies this phase. Figure 14a shows that the addition of nanoparticles can produce a steeper droplet size regression curve compared with pure HVO. Otherwise, micron size does not produce this effect. The droplet size evolution is closer to the HVO, indicating a lower burning rate, as will be addressed in the following results. The same observation occurs at the highest temperature, displayed in Figure 14b. The end of the droplet size evolution curves was not possible to determine experimentally due to the very small size of the droplet, thus it provided an estimation where micro-explosions appear by the number of frames until this phenomenon occurs. The reduction of the evaporation rate begins early in the higher temperature, in other words, the curvature of the normalized droplet diameter is more evident, e.g., in nanofuel, as shown in Figure 14b. The results also show that micro-explosions, which are marked in Figure 14, occur later for micron-sized particles suspended in HVO. The horizontal black line represented in Figure 14a,b corresponds to the instant $t/D_0^2 = 0.35$ s/mm^2 which is important to evaluate burning rate, as will be discussed later. The later appearance of micro-explosions in micron-sized particles can be related to findings reported in [18]. The authors stated that increasing the particle size increases the time to disruption. Additionally, the inter-particle distance increases and decreases the surface area, which can delay the micro-explosion and be responsible for the droplet size evolution difference compared with nanoparticles.

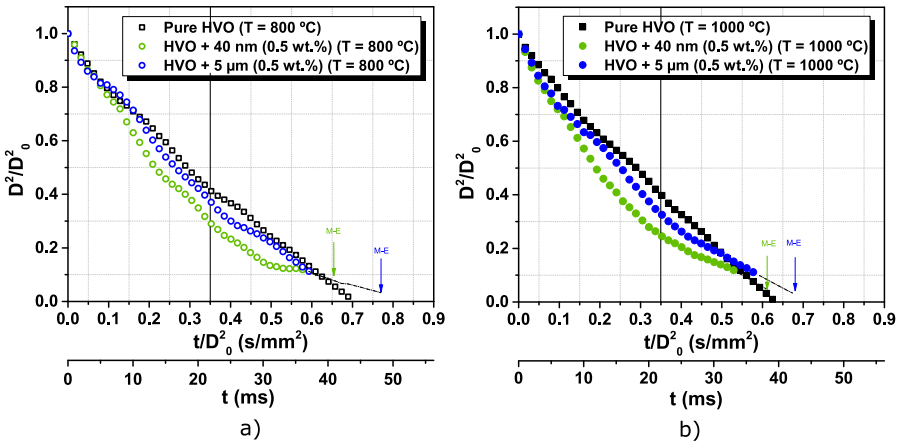

Figure 14. Square of the normalized droplet diameter as a function of the normalized time at (**a**) T = 800 °C and (**b**) T = 1000 °C.

Besides the fact that nano and micron-sized particles in HVO produce quite a different combustion behavior, in some operating conditions they enhance the burning rate. Figure 15 shows the temporal evolution of the burning rate for HVO + 40 nm (0.5 wt.%) and HVO + 5 µm (0.5 wt.%) at two furnace temperatures. At T = 800 °C, HVO + Al presents a few oscillations in the temporal evolution of burning rate, as shown in Figure 15a. This fact can be compared with pure HVO, which presents a more constant temporal evolution of the burning rate. However, the burning rate values are considerably higher in the early stages, HVO + 40 nm (0.5 wt.%) being the fuel with the highest values. Increasing the furnace temperature significantly increases the burning rate, as shown in Figure 15b. At T = 1000 °C, in the initial instants, the burning rate is substantially high. However, as time evolves, a significant reduction is noticed. This reduction is due to the high evaporation of liquid fuel that accumulates particles inside the droplet.

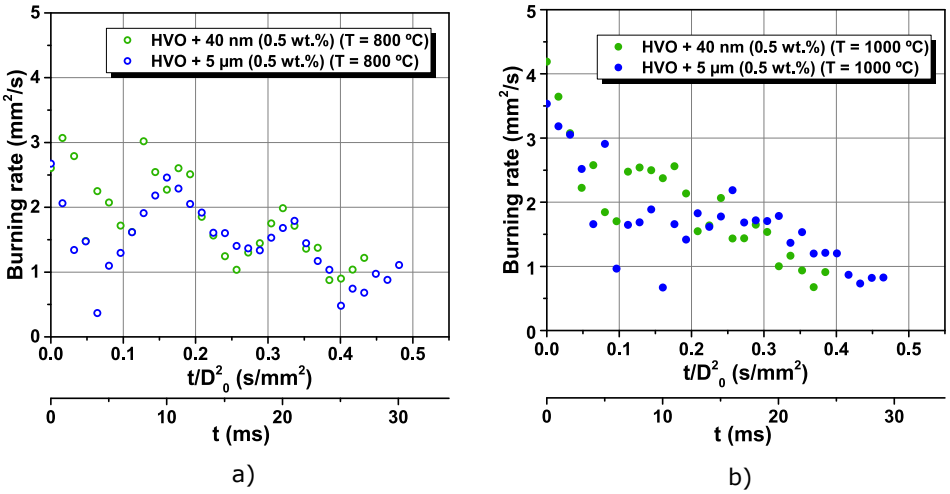

Figure 15. Temporal evolution of burning rate at (**a**) T = 800 °C and (**b**) T = 1000 °C.

The enhancement of the burning rate can be attributed to the radiation absorption [28,29]. The pure HVO is a transparent fuel, however when aluminum particles are added to the biofuel, they can behave approximately as a black body which consequently affects the radiation absorption. In addition, a parameter that can also influence the effectiveness of particles is thermal conductivity, as reported by [58,59]. Further studies covering experimental data on thermal conductivity and radiation absorption in liquid fuel with particles should be performed in order to evaluate and quantify how these influence combustion.

Figure 16 shows the burning rate of pure HVO and HVO + Al particles at two furnace temperatures (T = 800 °C and T = 1000 °C). A previously mentioned reduction of burning rate in T = 800 °C and T = 1000 °C during the final stage of the droplet's lifetime affect the fuel combustion in a distinct way.

Allied to this, disruptive burning phenomena were spotted in HVO + Al particles. Thus, to provide comparison results, the data between the furnace temperature and the fuels were acquired until t/D_0^2 = 0.35 s/mm^2. Pure HVO has the lowest burning rate, regardless of the furnace temperature. However, the addition of micron-sized particles does not significantly enhance the burning rate compared to the pure HVO. In this way, the most satisfactory results were achieved with the addition of nanoparticles. Considering until t/D_0^2 = 0.35 s/mm^2, an enhancement of approximately 24% was noticed for HVO + 40 nm (0.5 wt.%) in comparison with pure HVO at T = 1000 °C. Moreover, increasing the furnace temperature increases the burning rate for all the fuels tested in this investigation.

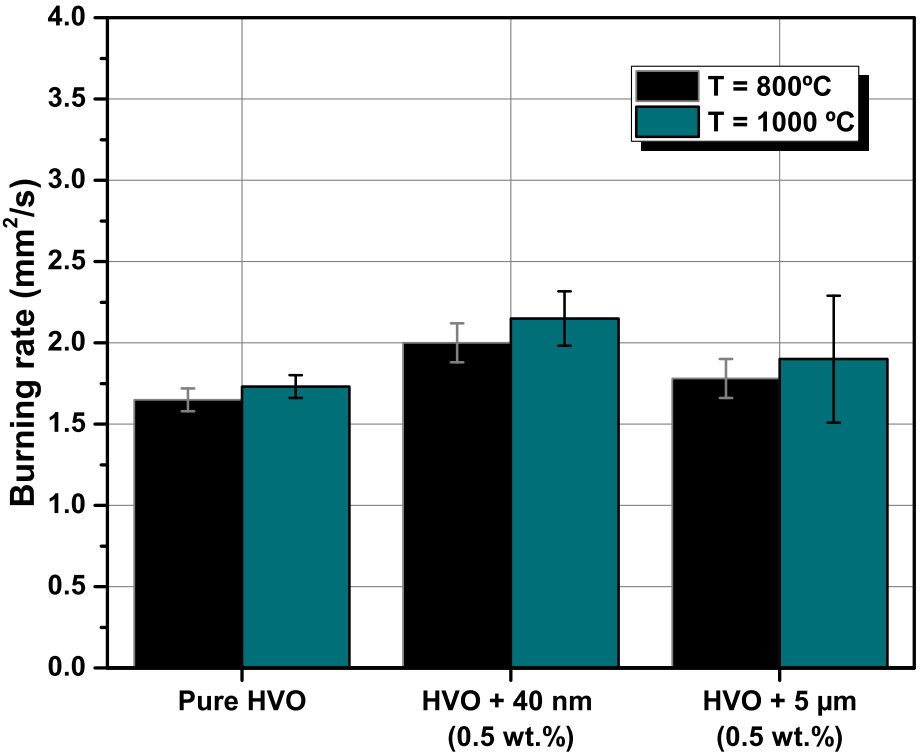

Figure 16. Burning rate for pure HVO and HVO + Al particles at T = 800 °C and T = 1000 °C.

4. Conclusions

The present work evaluates the combustion of Jet A-1, HVO, and HVO with aluminum particles. This experimental study provides insights regarding the combustion characteristics of the fuels in a falling droplet method under high furnace temperatures. In addition, it provides a comparison between conventional jet fuel and an aviation alternative fuel and the effect of aluminum particle size in the biofuel. The main conclusions from this work can be summarized as follows:

- Jet A-1 and HVO follow the D^2 law, and no disruptive burning event was detected. However, the difference in the flame intensity was noticed, being the Jet A-1, the fuel with brighter flames, due to the aromatic content in its composition.
- The addition of aluminum particles to the HVO promotes the occurrence of disruptive burning phenomena. Thus, micro-explosions pronounce the end of the droplet lifetime for HVO + Al particles, inducing secondary atomization.
- Higher furnace temperature leads to a higher burning rate for all fuels. Finally, considering the particle size range used in this work, the most encouraging results were obtained for HVO + 40 nm (0.5 wt.%), presenting the higher burning rate and lower lifetime.

Author Contributions: I.A.S.F.: Methodology, software, data curation, formal analysis, investigation, writing and original draft. M.A.A.M.: Conceptualization, resources, writing—review and editing, supervision, funding acquisition. A.S.O.H.M.: Conceptualization, methodology, resources, writing—review and editing, supervision, funding acquisition. A.R.R.S.: Conceptualization, methodology, validation, resources, writing—review and editing, supervision, funding acquisition. All authors have read and agreed to the published version of the manuscript.

Funding: Inês Ferrão acknowledges Fundação para a Ciência e Tecnologia (FCT) for the provision of Ph.D scholarship with the reference SFRH/BD/144688/2019. The present work was performed under the scope of the Laboratório Associado em Energia, Transportes e Aeronáutica (LAETA) and Laboratório de Robótica e Sistemas de Engenharia (LARSyS) activities and it was supported by FCT through the projects number UIDB/50022/2020 and UIDB/50009/2020. Authors would also like to acknowledge Fundação para a Ciência e Tecnologia for partially supporting this work through project PTDC/EME-SIS/2017.

Institutional Review Board Statement: Not applicable.

Informed Consent Statement: Not applicable.

Data Availability Statement: Not applicable.

Conflicts of Interest: The authors declare no conflict of interest.

Abbreviations

The following abbreviations are used in this manuscript:

Al	Aluminum
ASTM	American Society for Testing and Materials
BR	Burning Rate
DTF	Drop Tube Furnace
HVO	Hydrotread Vegetable Oil
HEFA	Hydroprocessed Esters and Fatty Acids
JF	Jet-Fuel
M-E	Micro-explosion

Appendix A.

Appendix A.1. Particles Images

Figure A1. Particle images: (**a**) 40 nm and (**b**) 5 µm.

Appendix A.2. Experimental Setup

Figure A2. Experimental setup (side view).

Figure A3. Experimental setup (front view).

References

1. Price, E.; Sigman, R. Combustion of aluminized solid propellants. In *Solid Propellant Chemistry, Combustion, and Motor Interior Ballistics (Progress in Astronautics and Aeronautics)*; American Institute of Aeronautics and Astronautics: Reston, VA, USA, 2000; Volume 185, pp. 663–687.
2. Berner, M.; Zarko, V.; Talawar, M. Nanoparticles of energetic materials: Synthesis and properties. *Combust. Explos. Shock Waves* **2013**, *49*, 625–647. [CrossRef]
3. Sundaram, D.; Yang, V.; Zarko, V.E. Combustion of nano aluminum particles. *Combust. Explos. Shock Waves* **2015**, *51*, 173–196. [CrossRef]
4. Dreizin, E.L. Metal-based reactive nanomaterials. *Prog. Energy Combust. Sci.* **2009**, *35*, 141–167. [CrossRef]
5. Choudhury, P.R. Slurry fuels. *Prog. Energy Combust. Sci.* **1992**, *18*, 409–427. [CrossRef]
6. Jones, M.; Li, C.H.; Afjeh, A.; Peterson, G. Experimental study of combustion characteristics of nanoscale metal and metal oxide additives in biofuel (ethanol). *Nanoscale Res. Lett.* **2011**, *6*, 246. [CrossRef]
7. Baek, S.W.; Cho, J.H. Microexplosion of aluminum slurry droplets. *Int. J. Heat Mass Transf.* **1999**, *42*, 4475–4486.
8. Wong, S.C.; Lin, A.C. Microexplosion mechanisms of aluminum/carbon slurry droplets. *Combust. Flame* **1992**, *89*, 64–76. [CrossRef]
9. Valiullin, T.; Vershinina, K.; Strizhak, P. Ignition of Slurry Fuel Droplets with Different Heating Conditions. *Energies* **2019**, *12*, 4553. [CrossRef]
10. Washburn, E.; Gross, M.; Smith, S.; Balachandar, S. Fundamental simulation of aluminum droplet combustion. In Proceedings of the 46th AIAA/ASME/SAE/ASEE Joint Propulsion Conference and Exhibit, Nashville, TN, USA, 25–28 July 2010; p. 6677.
11. Beckstead, M.; Liang, Y.; Pudduppakkam, K. Numerical simulation of single aluminum particle combustion. *Combust. Explos. Shock Waves* **2005**, *41*, 622–638. [CrossRef]
12. Liang, Y.; Beckstead, M. Numerical simulation of quasi-steady, single aluminum particle combustion in air. In Proceedings of the 36th AIAA Aerospace Sciences Meeting and Exhibit, Reno, NV, USA, 12–15 January 1998; p. 254.

13. Megaridis, C.M.; Sirignano, W.A. Numerical modeling of a slurry droplet containing a spherical particle. *J. Thermophys. Heat Transf.* **1993**, *7*, 110–119. [CrossRef]
14. Cravero, C.; Marogna, N.; Marsano, D. A Numerical Study of correlation between recirculation length and shedding frequency in vortex shedding phenomena. *WSEAS Trans. Fluid Mech* **2021**, *16*, 48–62. [CrossRef]
15. Shi, L.; Yang, G.; Yao, S. Large eddy simulation of flow past a square cylinder with rounded leading corners: A comparison of 2D and 3D approaches. *J. Mech. Sci. Technol.* **2018**, *32*, 2671–2680. [CrossRef]
16. Fan, X.; Lu, X. Numerical simulation of single droplet combustion characteristics in high temperature convection environment. In *IOP Conference Series: Earth and Environmental Science*; IOP Publishing: Bristol, UK, 2019; Volume 267, p. 062050.
17. Shinjo, J.; Xia, J.; Ganippa, L.; Megaritis, A. Physics of puffing and microexplosion of emulsion fuel droplets. *Phys. Fluids* **2014**, *26*, 103302. [CrossRef]
18. Takahashi, F.; Heilweil, I.; Dryer, F. Disruptive burning mechanism of free slurry droplets. *Combust. Sci. Technol.* **1989**, *65*, 151–165. [CrossRef]
19. Yetter, R.A.; Risha, G.A.; Son, S.F. Metal particle combustion and nanotechnology. *Proc. Combust. Inst.* **2009**, *32*, 1819–1838. [CrossRef]
20. Basu, S.; Miglani, A. Combustion and heat transfer characteristics of nanofluid fuel droplets: A short review. *Int. J. Heat Mass Transf.* **2016**, *96*, 482–503. [CrossRef]
21. Tyagi, H.; Phelan, P.E.; Prasher, R.; Peck, R.; Lee, T.; Pacheco, J.R.; Arentzen, P. Increased hot-plate ignition probability for nanoparticle-laden diesel fuel. *Nano Lett.* **2008**, *8*, 1410–1416. [CrossRef]
22. Gan, Y.; Qiao, L. Combustion characteristics of fuel droplets with addition of nano and micron-sized aluminum particles. *Combust. Flame* **2011**, *158*, 354–368. [CrossRef]
23. Javed, I.; Baek, S.W.; Waheed, K. Effects of dense concentrations of aluminum nanoparticles on the evaporation behavior of kerosene droplet at elevated temperatures: The phenomenon of microexplosion. *Exp. Therm. Fluid Sci.* **2014**, *56*, 33–44. [CrossRef]
24. Ojha, P.K.; Maji, R.; Karmakar, S. Effect of crystallinity on droplet regression and disruptive burning characteristics of nanofuel droplets containing amorphous and crystalline boron nanoparticles. *Combust. Flame* **2018**, *188*, 412–427. [CrossRef]
25. Singh, G.; Esmaeilpour, M.; Ratner, A. Effect of carbon-based nanoparticles on the ignition, combustion and flame characteristics of crude oil droplets. *Energy* **2020**, *197*, 117227. [CrossRef]
26. Tanvir, S.; Qiao, L. Effect of addition of energetic nanoparticles on droplet-burning rate of liquid fuels. *J. Propuls. Power* **2015**, *31*, 408–415. [CrossRef]
27. Tanvir, S.; Biswas, S.; Qiao, L. Evaporation characteristics of ethanol droplets containing graphite nanoparticles under infrared radiation. *Int. J. Heat Mass Transf.* **2017**, *114*, 541–549. [CrossRef]
28. Emekwuru, N.G. Nanofuel droplet evaporation processes. *J. Indian Inst. Sci.* **2019**, *99*, 43–58. [CrossRef]
29. Gan, Y.; Qiao, L. Radiation-enhanced evaporation of ethanol fuel containing suspended metal nanoparticles. *Int. J. Heat Mass Transf.* **2012**, *55*, 5777–5782. [CrossRef]
30. Ghamari, M.; Ratner, A. Combustion characteristics of colloidal droplets of jet fuel and carbon based nanoparticles. *Fuel* **2017**, *188*, 182–189. [CrossRef]
31. Xiu-tian feng, E.; Zhi, X.; Zhang, Y.; Li, C.; Zou, J.J.; Zhang, X.; Wang, L. Jet fuel containing ligand-protecting energetic nanoparticles: A case study of boron in JP-10. *Chem. Eng. Sci.* **2015**, *129*, 9–13.
32. Ng, K.S.; Farooq, D.; Yang, A. Global biorenewable development strategies for sustainable aviation fuel production. *Renew. Sustain. Energy Rev.* **2021**, *150*, 111502. [CrossRef]
33. Hemighaus, G.; Boval, T.; Bacha, J.; Barnes, F.; Franklin, M.; Gibbs, L.; Hogue, N.; Jones, J.; Lesnini, D.; Lind, J.; et al. *Aviation Fuels Technical Review*; Chevron Products Company: San Ramon, CA, USA, 2006.
34. Rochelle, D.; Najafi, H. A review of the effect of biodiesel on gas turbine emissions and performance. *Renew. Sustain. Energy Rev.* **2019**, *105*, 129–137. [CrossRef]
35. Yilmaz, N.; Atmanli, A. Sustainable alternative fuels in aviation. *Energy* **2017**, *140*, 1378–1386. [CrossRef]
36. Hari, T.K.; Yaakob, Z.; Binitha, N.N. Aviation biofuel from renewable resources: Routes, opportunities and challenges. *Renew. Sustain. Energy Rev.* **2015**, *42*, 1234–1244. [CrossRef]
37. Patruno, A.; Amicarelli, V.; Lagioia, G. Aviation Fuel Evolution: A Review. 2017. Available online: www.asecu.gr/files/13th/conf_files/The-Aviation-Fuel-Evolution-A-Review.pdf (accessed on 5 January 2022).
38. Blakey, S.; Rye, L.; Wilson, C.W. Aviation gas turbine alternative fuels: A review. *Proc. Combust. Inst.* **2011**, *33*, 2863–2885. [CrossRef]
39. Yang, J.; Xin, Z.; Corscadden, K.; Niu, H. An overview on performance characteristics of bio-jet fuels. *Fuel* **2019**, *237*, 916–936. [CrossRef]
40. Pizziol, B.; Costa, M.; Panão, M.O.; Silva, A. Multiple impinging jet air-assisted atomization. *Exp. Therm. Fluid Sci.* **2018**, *96*, 303–310. [CrossRef]
41. Pacheco, G.; Silva, A.; Costa, M. Single-Droplet Combustion of Jet A-1, Hydroprocessed Vegetable Oil, and Their Blends in a Drop-Tube Furnace. *Energy Fuels* **2021**, *35*, 7232–7241. [CrossRef]
42. Simacek, P.; Soucek, I.; Pospisil, M.; Vrtiska, D.; Kittel, H. Impact of hydrotreated vegetable oil and biodiesel on properties in blends with mineral diesel fuel. *Therm. Sci.* **2019**, *23*, 1769–1777. [CrossRef]
43. Wang, L.; Chen, H.; Witharana, S. Rheology of nanofluids: A review. *Recent Pat. Nanotechnol.* **2013**, *7*, 232–246. [CrossRef]

44. Arshad, A.; Jabbal, M.; Yan, Y.; Reay, D. A review on graphene based nanofluids: Preparation, characterization and applications. *J. Mol. Liq.* **2019**, *279*, 444–484. [CrossRef]
45. Moita, A.S.; Laurência, C.; Ramos, J.A.; Prazeres, D.M.F.; Moreira, A.L.N. Dynamics of droplets of biological fluids on smooth superhydrophobic surfaces under electrostatic actuation. *J. Bionic Eng.* **2016**, *13*, 220–234. [CrossRef]
46. Tanvir, S.; Qiao, L. Surface tension of nanofluid-type fuels containing suspended nanomaterials. *Nanoscale Res. Lett.* **2012**, *7*, 226. [CrossRef]
47. Clayton, R.; Back, L. Physical and chemical characteristics of cenospheres from the combustion of heavy fuel oil. *J. Eng. Gas Turbines Power.* **1989**, 679–684. [CrossRef]
48. Jiang, L.; Elbaz, A.M.; Guida, P.; Al-Noman, S.M.; AlGhamdi, I.A.; Saxena, S.; Roberts, W.L. Cenosphere formation during single-droplet combustion of heavy fuel oil. *Energy Fuels* **2019**, *33*, 1570–1581. [CrossRef]
49. Ferrão, I.A.; Silva, A.R.; Moita, A.S.; Mendes, M.A.; Costa, M.M. Combustion characteristics of a single droplet of hydroprocessed vegetable oil blended with aluminum nanoparticles in a drop tube furnace. *Fuel* **2021**, *302*, 121160. [CrossRef]
50. Stöhr, M.; Ruoff, S.; Rauch, B.; Meier, W.; Le Clercq, P. Droplet vaporization for conventional and alternative jet fuels at realistic temperature conditions: Systematic measurements and numerical modeling. *Proc. Combust. Inst.* **2021**, *38*, 3269–3276. [CrossRef]
51. Liu, Y.C.; Savas, A.J.; Avedisian, C.T. The spherically symmetric droplet burning characteristics of Jet-A and biofuels derived from camelina and tallow. *Fuel* **2013**, *108*, 824–832. [CrossRef]
52. Buffi, M.; Valera-Medina, A.; Marsh, R.; Pugh, D.; Giles, A.; Runyon, J.; Chiaramonti, D. Emissions characterization tests for hydrotreated renewable jet fuel from used cooking oil and its blends. *Appl. Energy* **2017**, *201*, 84–93. [CrossRef]
53. Chishty, W.A.; Davison, C.R.; Bird, J.; Chan, T.; Cuddihy, K.; McCurdy, M.; Barton, P.; Krasteva, A.; Poitras, P. Emissions assessment of alternative aviation fuel at simulated altitudes. In Proceedings of the Turbo Expo: Power for Land, Sea, and Air, Vancouver, BC, Canada, 6–10 June 2011; Volume 54617, pp. 51–61.
54. Gan, Y.; Lim, Y.S.; Qiao, L. Combustion of nanofluid fuels with the addition of boron and iron particles at dilute and dense concentrations. *Combust. Flame* **2012**, *159*, 1732–1740. [CrossRef]
55. Bennewitz, J.W.; Badakhshan, A.; Talley, D.G. Combustion characteristics of suspended hydrocarbon fuel droplets with various nanoenergetic additives. *Combust. Sci. Technol.* **2021**, *193*, 2111–2136. [CrossRef]
56. Guerieri, P.M.; DeCarlo, S.; Eichhorn, B.; Connell, T.; Yetter, R.A.; Tang, X.; Hicks, Z.; Bowen, K.H.; Zachariah, M.R. Molecular aluminum additive for burn enhancement of hydrocarbon fuels. *J. Phys. Chem. A* **2015**, *119*, 11084–11093. [CrossRef]
57. Li, H.; Rosebrock, C.D.; Wu, Y.; Wriedt, T.; Mädler, L. Single droplet combustion of precursor/solvent solutions for nanoparticle production: Optical diagnostics on single isolated burning droplets with micro-explosions. *Proc. Combust. Inst.* **2019**, *37*, 1203–1211. [CrossRef]
58. Kim, D.M.; Baek, S.W.; Yoon, J. Ignition characteristics of kerosene droplets with the addition of aluminum nanoparticles at elevated temperature and pressure. *Combust. Flame* **2016**, *173*, 106–113. [CrossRef]
59. Aboalhamayie, A.; Festa, L.; Ghamari, M. Evaporation rate of colloidal droplets of jet fuel and carbon-based nanoparticles: Effect of thermal conductivity. *Nanomaterials* **2019**, *9*, 1297. [CrossRef] [PubMed]